Split-ring-based metamaterial for far-field subwavelength focusing based on time reversal*

Huang Hai-Yan(黄海燕)†, Ding Shuai(丁 帅), Wang Bing-Zhong(王秉中), and Zang Rui(臧 锐)

Institute of Applied Physics, University of Electronic Science and Technology of China, Chengdu 610054, *China*

(Received 22 May 2013; revised manuscript received 1 November 2013; published online 10 April 2014)

In this paper, split-ring-based metamaterial sheets are designed for the purpose of achieving far-field subwavelength focusing, with the aid of a time-reversal technique. The metamaterial sheets are inserted into a subwavelength array consisting of four element antennas, with the element spacing being as small as 1/15 of a wavelength. Experiments are performed to investigate the effect of the metamaterial sheets on the focusing resolution. The results demonstrate that in the presence of the metamaterial sheets, the subwavelength array exhibits the ability to achieve super-resolution focusing, while there is no super-resolution focusing without the metamaterial sheets. Further investigation shows that the metamaterial sheets are contributive to achieving super-resolution by weakening the cross-correlations of the channel impulse responses between the array elements.

Keywords: time-reversal, metamaterial, subwavelength focusing

PACS: 41.20.Jb, 42.25.Bs, 84.40.Ba **DOI:** 10.1088/1674-1056/23/6/064101

1. Introduction

In recent years, electromagnetic metamaterials have received a lot of attention due to their extraordinary physical properties which do not exist in natural materials.[1–5] In addition to their wide applications in electromagnetic engineering, metamaterials also have found a use in subwavelength resolution imaging.[6–8] Because of the diffraction limit, in a traditional microwave imaging system, the peak voltages received by two adjacent antennas tend to be identical, when they are placed less than half a wavelength apart. This phenomenon limits the imaging resolution to half a wavelength. With advances in near-field optics research, the subwavelength resolution imaging would be possible if more evanescent waves from the source are captured. There is a fact that evanescent waves contain the fine structure information about the source object, and therefore the more the evanescent waves are captured, the better the imaging resolution will be. Due to their structure characteristics, metamaterials can play a role in exciting and propagating evanescent waves. A grating-like plate with a patterned surface with a focusing resolution as high as 1/20 λ in the near-field zone was presented.[6] A metallic wire array is another structure widely used to obtain subwavelength imaging.[7,8] As pointed out by Belov, the metallic wire array can provide canalizations for evanescent waves to propagate through, leading to an imaging resolution on the subwavelength scale. Owing to the exponential decay of evanescent wave intensity along its propagating distance, the aforementioned subwavelength imaging is restricted in the near-field zone.

Compared with near-field subwavelength imaging, far-field subwavelength imaging is especially agreeable in applications, such as detecting, energy transmission, and multiple input multiple output (MIMO) antenna array designing. Far-field super-resolution imaging usually means focusing with a lateral resolution better than half a wavelength. Over the past decades, efforts have been made to acquire far-field super-resolution imaging.[9–13] A metal wire array combined with the time-reversal (TR) technique is feasible to achieve super-resolution imaging in the far-field zone.[9,10] Resolution as high as one-thirtieth of a wavelength has been realized by Lerosey, etc., through adding scatters placed in the near-field region and using the TR technique.[13] Further investigations indicate that the near-field scatters conduce to the generation of evanescent waves, and enable the conversion between propagating waves and evanescent waves. Besides, the space-time focusing property of the TR electromagnetic wave is also helpful to improve imaging resolution.[14–19] Later reports indicate that the near-field scatters can be replaced by micro-patterns-etched array elements. Subwavelength arrays composed of such array elements, which achieve the super-resolution characteristic with the TR technique, were reported.[20,21] Although there have been many reports of experiments on far-field super-resolution focusing, the effect of the scatters on imaging resolution is not studied thoroughly, and the mechanism of TR super-resolution focusing is not very clear either. In this paper, split-ring-based metamaterial sheets are used to obtain far-field super-resolution focusing with the aid of the TR technique. Experiments and analysis are also carried out

*Project supported by the National Natural Science Foundation of China (Grant Nos. 61071031, 61331007, and 61107018), the Research Fund for the Doctoral Program of Higher Education of China (Grant Nos. 20100185110021 and 20120185130001), the Fundamental Research Funds for the Central Universities, China (Grant No. E02205205), and the Project ITR1113, China.

†Corresponding author. E-mail: haiyanhuang123@yahoo.com

© 2014 Chinese Physical Society and IOP Publishing Ltd

to investigate the effects which influence the resolution performance.

2. Influence of split-ring-based metamaterial sheets on channel response

The metamaterial sheets are used as isolators to separate the element antennas. The details of the matematerial sheets are shown in Fig. 1. The structure is a 15×15 metal split-ring array printed on a 100 mm×100 mm×1 mm substrate with a dielectric constant $\varepsilon_r = 2.33$. The dimensions of the unit cell are as follows: $g = 1$ mm, $r = 2$ mm, $d = 6.5$ mm, and $R = 3$ mm. An array composed of four traditional wideband antennas is employed as a receiving array, as shown in Fig. 2(a). The distance d' between two adjacent antennas is 5 mm. The wavelength λ_0 corresponding to the central operating frequency is 75 mm. Thus the distance between two adjacent antennas is 1/15 λ_0 , which is much less than half a wavelength. Figure 2(b) illustrates the element antennas of the array isolated by the proposed metamaterial sheets.

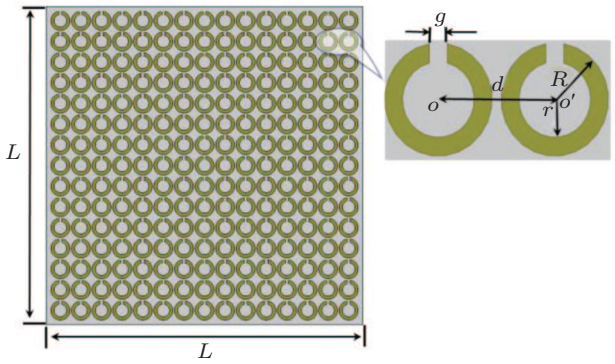


Fig. 1. (color online) Details of a split-ring-based metamaterial sheet.

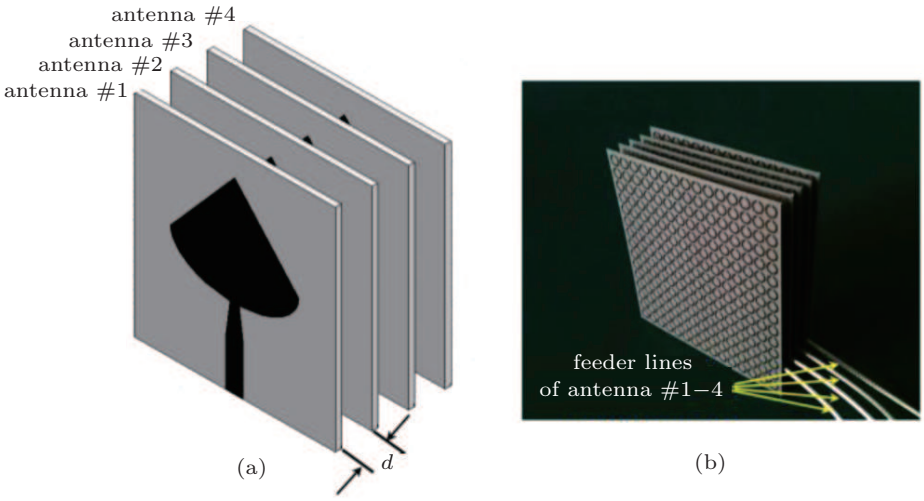


Fig. 2. (color online) (a) Sub-wavelength array. (b) Element antennas of sub-wavelength array isolated by metamaterial sheets.

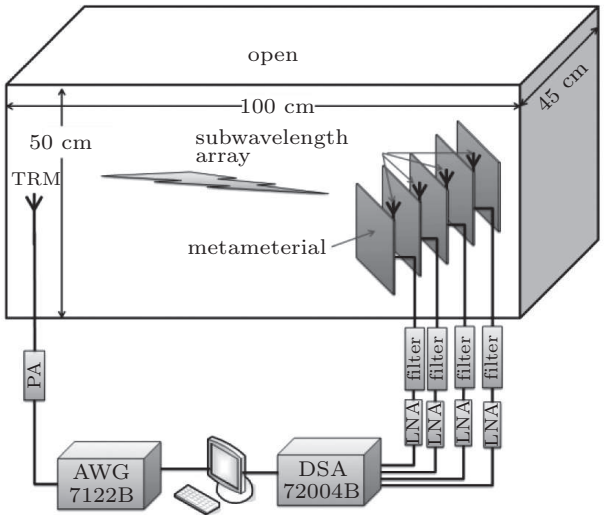


Fig. 3. Experiment schematic plot.

In order to investigate the influence of the split-ring-based metamaterial sheets on the receiving channel impulse responses, experiments are carried out. The experiment schematic plot is shown in Fig. 3. The experiments are performed in a metal box with the upper side open. The geometry size of the box is 100 cm×50 cm×45 cm. The spacing between the time-reversal mirror (TRM) antenna and the subwavelength antenna array is 70 cm. A modulated Gaussian signal $x(t)$ with a central frequency of 4 GHz and an operation bandwidth of 2 GHz–6 GHz is utilized as a test signal.

The experiment steps are as follows. Firstly, the test pulse signal $x(t)$ is generated by the arbitrary waveform generator AWG7122B and fed to the TRM antenna to be emitted. Secondly, the signal received by each element of the subwavelength array is recorded by the DSA 72004B and denoted as $y_i(t)$ $(i = 1,2,3,4)$. Thirdly, the channel response $H_i(t)$ between the TRM antenna and the i-th element antenna is extracted by the CLEAN algorithm.[22] Fourthly, we remove the metamaterial sheets, repeat experiment from step 1 to step 3, and then extract the channel response $H_i'(t)$ for the case without metamaterial sheets.

Figure 4 shows $H_i'(t)$, the receiving channel impulse response of the i-th element antenna. Figure 5 gives $H_i'(t)$, the receiving channel impulse response of the i-th element antenna without metamaterial sheets. From Figs. 4 and 5, it can be seen that in the presence of the metamatial sheets, the impulse responses have more multipath components than in the absence of metamatial sheets. The channel impulse responses in Fig. 4 are different from those in Fig. 5. Specifically speaking, the multipath delays and multipath amplitudes in Fig. 4(a) corresponding to antenna #1 differ from those in Fig. 4(b) corresponding to antenna #2. However, these differences are not obvious between Fig. 5(a) and Fig. 5(b). Figures 4 and 5 reveal that the metamaterial sheets certainly change the wave propagation. In order to explain the correlations of the channel impulse responses quantitatively, the correlation matrices are calculated for the two cases with and without metamaterial sheets, respectively.

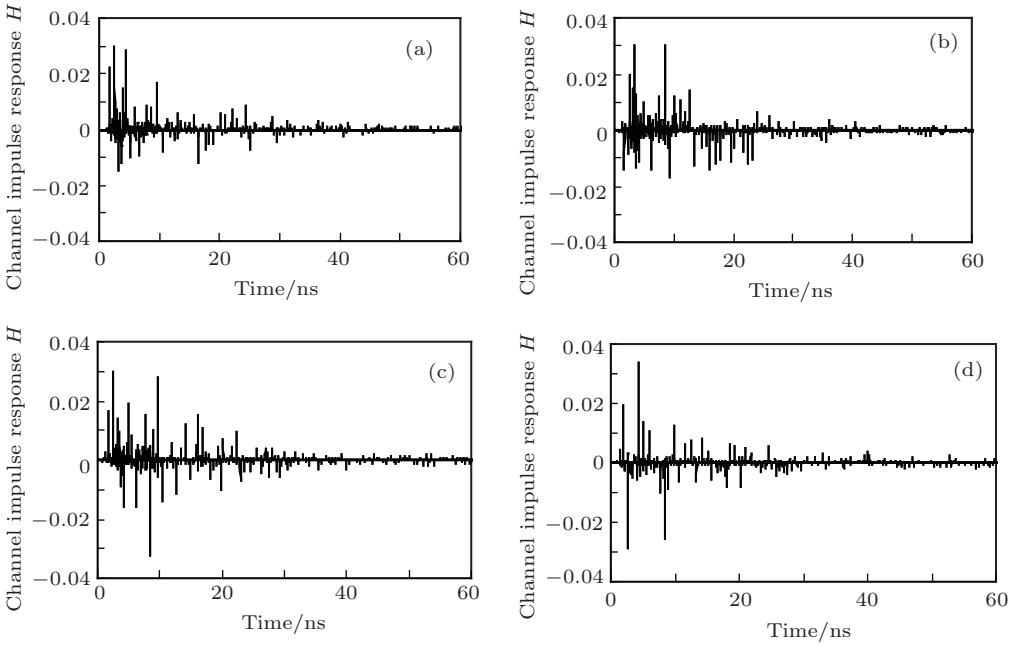


Fig. 4. Channel impulse response of each antenna with the metamaterial sheets. (a) Channel impulse response between antenna #1 and the TRM antenna. (b) Channel impulse response between antenna #2 and the TRM antenna. (c) Channel impulse response between antenna #3 and the TRM antenna. (d) Channel impulse response between antenna #4 and the TRM antenna.

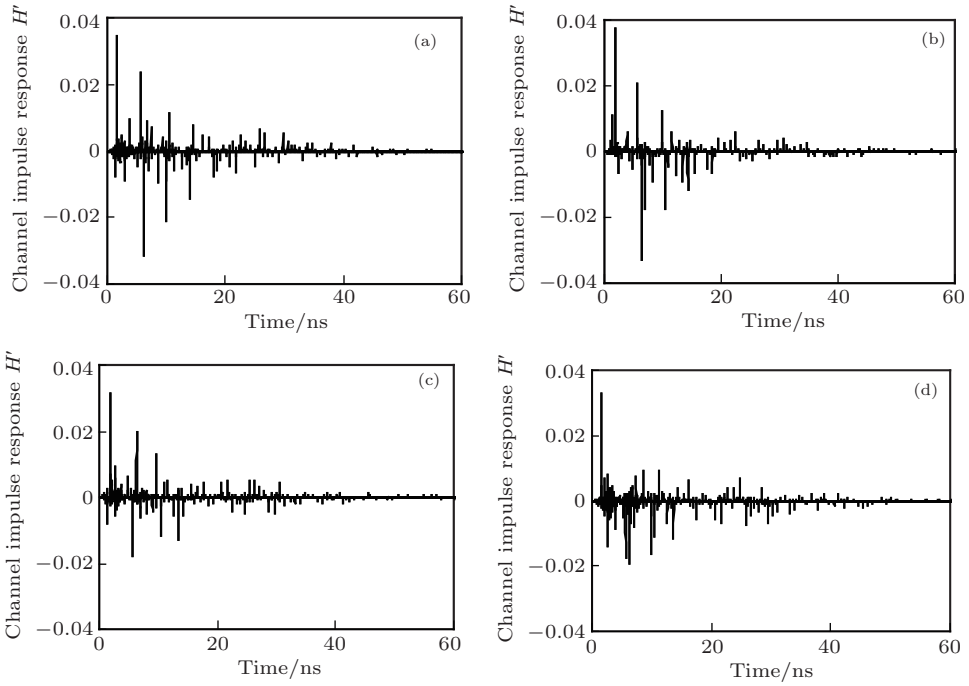


Fig. 5. Channel impulse response of each antenna without metamaterial sheets. (a) Channel impulse response between antenna #1 and the TRM antenna. (b) Channel impulse response between antenna #2 and the TRM antenna. (c) Channel impulse response between antenna #3 and the TRM antenna. (d) Channel impulse response between antenna #4 and the TRM antenna.

In the presence of the split-ring-based matematerial sheets, the correlation coefficient matrix of channel responses is given as follows:

$$\rho = \begin{bmatrix} 1 & 0.44 & 0.38 & 0.23 \\ 0.44 & 1 & 0.42 & 0.32 \\ 0.38 & 0.42 & 1 & 0.24 \\ 0.23 & 0.32 & 0.24 & 1 \end{bmatrix}. \quad (1)$$

The correlation coefficient matrix of the channel response without the split-ring-based matematerial sheets is written as follows:

$$\rho' = \begin{bmatrix} 1 & 0.84 & 0.78 & 0.38 \\ 0.84 & 1 & 0.73 & 0.51 \\ 0.78 & 0.73 & 1 & 0.57 \\ 0.38 & 0.51 & 0.57 & 1 \end{bmatrix}. \quad (2)$$

From Eqs. (1) and (2), it can be found that the split-ring-based matematerial sheets can considerably reduce the cross-correlation coefficients of the channel responses. It is well known that when two antennas get too close, say, smaller than half a wavelength, the receiving channel responses of these two antennas are highly correlated. Therefore, the resolution of a conventional antenna array is limited by the diffraction limit. The capacity of the split-ring-based metamaterial sheets to reduce the correlations between element antennas implies that they can be used to improve the focusing performance. We conduct further experiments associated with the TR technique to explore the far-field subwavelength focusing implementing the proposed metamaterial sheets.

3. Effect of split-ring-based metamaterial sheets on far-field subwavelength focusing

Generally, a typical TR experiment contains the following steps: firstly, a target antenna emits a test signal, then the test signal is received by a TRM antenna; secondly, the received signal is time-reversed and re-emitted by the TRM antenna; thirdly, the time-reversed signal is received by the target antenna and the eavesdropping antennas. Through comparing the received signal of the target antenna with those of the eavesdropping antennas, the resolution can be determined. However, there is a fact that the arbitrary waveform generator AWG7122B could only transmit signals. On the other hand, the digital series analyzer DSA72004B could only receive signals. In order to avoid changing the connection cables from AWG7122B to DSA72004B constantly, which is inconvenient and would influence the experiment results, the time-reversal mirror is always connected with AWG7122B and the subwavelength array is always connected with DSA72004B. According to the reciprocity of linear time invariant systems, this arrangement is appropriate. In other words, the transmitting process in which the time-reversal mirror antenna serves as a transmitting antenna and antenna #1 serves as a receiving antenna, is equivalent to the process in which antenna #1 serves as a transmitting antenna and the time-reversal mirror antenna serves as a receiving antenna. The steps of our time-reversal experiment are conducted as follows. Firstly, we assume that antenna #1 in the subwavelength array is the target antenna while the rest of the antennas in the subwavelength array are eavesdropping antennas; a modulation Gaussian signal $x(t)$ is transmitted by the time-reversal mirror antenna. Secondly, we record the signal received by the i-th antenna of the subwavelength array as $y_i(t)$ $(i = 1,2,3,4)$. Thirdly, we reverse the signal $y_1(t)$ received by antenna #1 in the time domain, obtaining $y_1(-t)$, which is then generated by AWG7122B and fed into the time-reversal mirror antenna to be re-emitted. Fourthly, we record the final signal received by each antenna as $f_i^{\mathrm{TR}}(t)$ $(i = 1,2,3,4)$. Fifthly, let antenna #2, antenna #3, and antenna #4 be the target antenna in turn, and repeat the above experiment steps 1–4. Sixthly, we remove the metamaterial sheets, and repeat the same experiment steps 1–5.

Figure 6 shows the final signals $f_i^{\mathrm{TR}}(t)$, with the metamaterial sheets being present and antenna #1 serving as the target antenna. From Fig. 6, it is obvious that due to the existence of the metamaterial sheets and the aid of the time-reversal technique, the target antenna receives the highest peak voltage while the other antenna elements receive the signals that have lower peak voltages (much less than half of that received by antenna #1).

As a comparison, the case without metamaterial sheets is also investigated. Figure 7 shows the focusing performance without the metamaterial sheets, with antenna #1 serving as the target antenna. As shown in Fig. 7, due to the high correlation, the received signals by antenna #1, antenna #2, and antenna #3 have similar peak voltages. For antenna #4, the distance from it to antenna #1 is further than to the other two, and therefore the peak voltage received by antenna #4 is the lowest. It can also be found that the peak voltage received by antenna #1 in Fig. 7 is higher than its counterpart in Fig. 6. Simulations in the CST microwave studio provide the reason responsible for this phenomenon. The existence of metamaterial sheets changes the impedance of the subwavelength array, resulting in impedance mismatching, which gives rise to the decrease in the peak amplitudes of the final received signals.

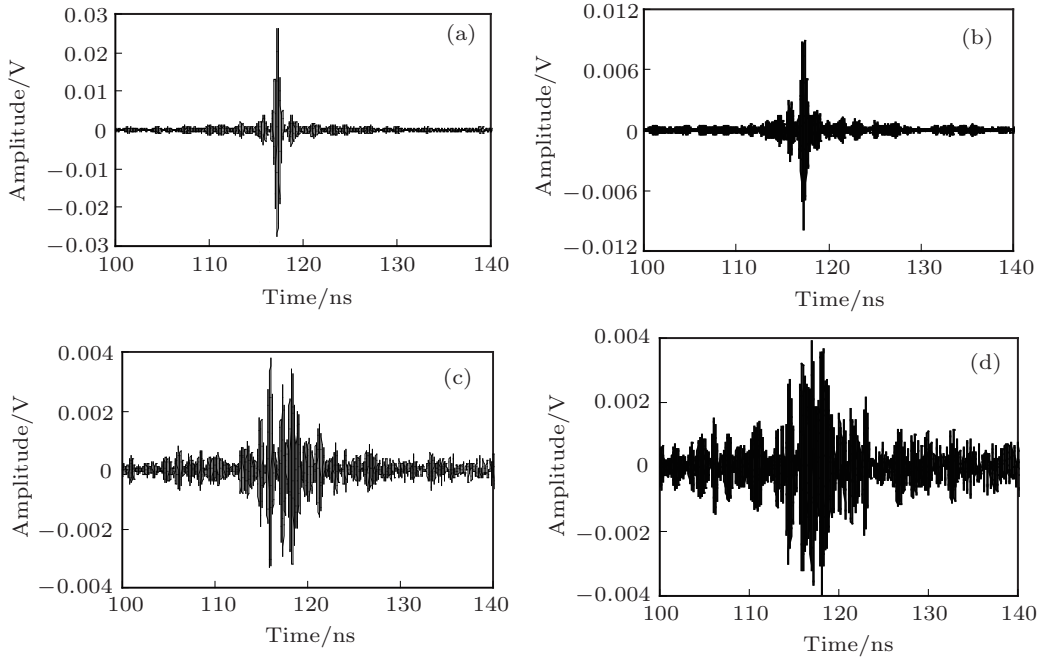


Fig. 6. Received TR signals at four element antennas of a subwavelength array with metamaterial sheets being present and antenna #1serving as the target antenna. (a) Signal received by antenna #1. (b) Signal received by antenna #2. (c) Signal received by antenna #3. (d) Signal received by antenna #4.

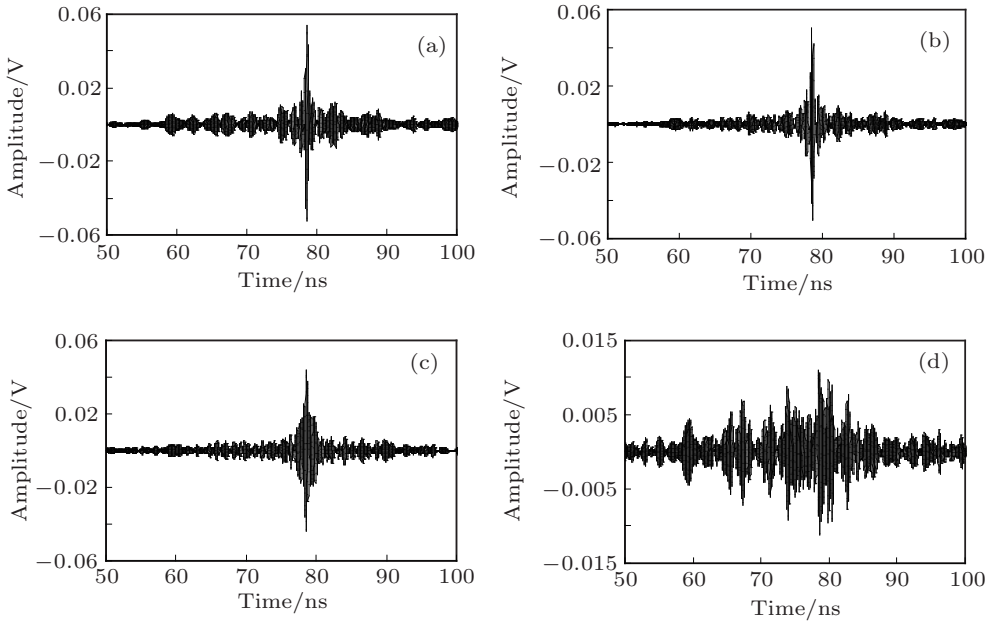


Fig. 7. Received TR signals at four element antennas of a subwavelength array without metamaterial sheets, and with antenna #1 serving as the target antenna. (a) Signal received by antenna #1. (b) Signal received by antenna #2. (c) Signal received by antenna #3. (d) Signal received by antenna #4.

Figure 8 depicts the normalized peak voltages received by the antenna elements in the presence of metamaterial sheets, with antenna #1, antenna #2, antenna #3, and antenna #4 used as the target antenna in sequence. Generally, when the element spacing is less than half a wavelength, and the peak amplitude of the received signal of the target antenna is twice as big as those of the eavesdropping antennas, the array is considered to have a super-resolution focusing characteristic.[20] As shown in Fig. 8, with the assistance of the proposed metamaterial sheets, the subwavelength array exhibits the super-resolution characteristic in the far-field zone. From Fig. 8, it is clear that the maximum peak voltage can be received only by the target antenna.

Figure 9 shows the normalized peak voltages of the received signals at the four antennas without the metamaterial sheets, using antenna #1, antenna #2, antenna #3, and antenna

#4 as the target antenna in turn. As shown in Fig. 9, even with the aid of the TR technique, the subwavelength antenna array does not have the super-resolution characteristic in the absence of the metamaterial sheets.

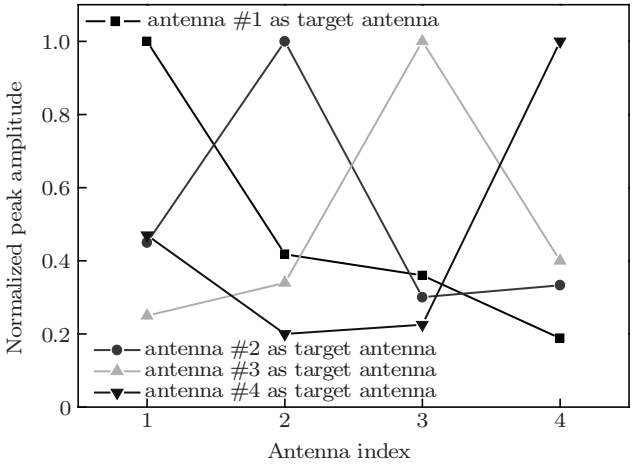


Fig. 8. Normalized peak voltages of the received TR signals at four element antennas of a subwavelength array with metamaterial sheets, using antenna #1, antenna #2, antenna #3, and antenna #4 as the target antenna in sequence.

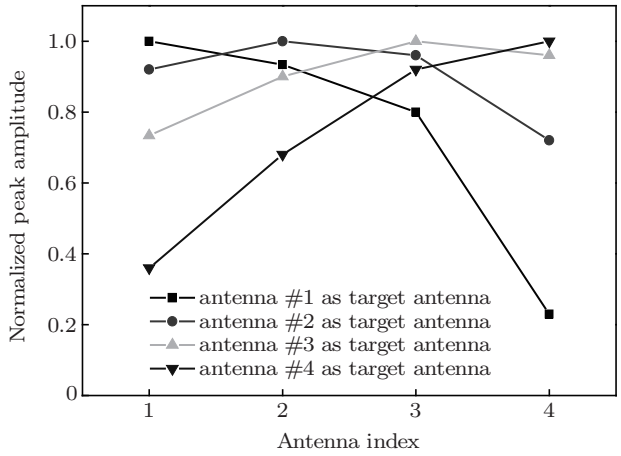


Fig. 9. Normalized peak voltages of the received TR signals at four element antennas of a subwavelength array without metamaterial sheets, using antenna #1, antenna #2, antenna #3, and antenna #4 as the target antenna in sequence.

4. Theoretical analysis

In order to thoroughly comprehend the effect of metamaterial sheets on the focusing performance, the mathematical expressions of the focusing process of a TR electromagnetic wave are deduced. For simplicity and convenience, we only take two antenna elements, antenna #1 and antenna #2, into account when we deduce the expressions; no doubt the other two antenna elements have similar expressions. Antenna #1 is set as the target antenna in the derivation.

4.1. Analysis in frequency domain

The impulse responses between the TRM antenna and the element antennas can be written in the following forms:

$$H_1 = |H_1|\,\mathrm{e}^{\mathrm{j}\theta_1}, \tag{3}$$

$$H_2 = |H_2|\,\mathrm{e}^{\mathrm{j}\theta_2}, \tag{4}$$

where $|H_1|$ and $|H_2|$ are the amplitudes of the channel responses of antenna #1 and antenna #2, respectively, and θ_1 and θ_2 are the corresponding phases of the channel responses.

A test signal $X\,\mathrm{e}^{\mathrm{j}x}$ is sent by the TRM antenna, X and x corresponding to the amplitude and the phase of the signal respectively. If the phase of the test signal is zero, the signals received by antenna #1 and antenna #2 can be expressed as follows:

$$\boldsymbol{F} = \begin{vmatrix} X|H_1|\,\mathrm{e}^{\mathrm{j}\theta_1} \\ X|H_2|\,\mathrm{e}^{\mathrm{j}\theta_2} \end{vmatrix}. \tag{5}$$

Because a time-reversal in the time domain is equivalent to a phase conjugation in the frequency domain, the signal received by antenna #1 is phase-conjugated and then is emitted by the TRM antenna again. The final signals received by the antenna elements are as follows:

$$\boldsymbol{F}^{\mathrm{TR}} = \begin{vmatrix} X|H_1|^2 \\ X|H_1||H_2|\,\mathrm{e}^{\mathrm{j}(\theta_2-\theta_1)} \end{vmatrix}. \tag{6}$$

From Eq. (6), it can be known that phase conjugation can only compensate the phase of the signal received by the target antenna, and for the non-target antenna, there is no phase conjugation. Applying the inverse Fourier transform to the received signals gives the received signals in the time domain, which are expressed as follows:

$$f_1^{\mathrm{TR}}(t) = \int_{-\infty}^{+\infty} X|H_1|^2\,\mathrm{e}^{\mathrm{j}\omega t}\,\mathrm{d}\omega, \tag{7}$$

$$f_2^{\mathrm{TR}}(t) = \int_{-\infty}^{+\infty} X|H_1||H_2|\,\mathrm{e}^{\mathrm{j}(\theta_2-\theta_1+\omega t)}\,\mathrm{d}\omega. \tag{8}$$

From Eqs. (7) and (8), it is clear that for the target antenna, the TR technique compensates for the phase of the received signal at each frequency. Therefore, the resulting signal in the time domain is the in-phase superposition of the components at each frequency. For the non-target antenna, namely antenna #2, the superposition is associated with the relation between θ_1 and θ_2. Because θ_1 varies at each frequency, and so does θ_2, the phase difference, i.e., θ_1–θ_2 is not linearly related to the frequency. Therefore, there is no such point in the time domain at which all the components are in-phase superposed, which results in a smaller peak voltage for the non-target antenna. The split-ring-based sheets play a role in facilitating the coupling between the sheets and the subwavelength array elements, which reduces the correlation of the channel responses, and ultimately improves the resolution performance.

4.2. Analysis in time domain

The received signals at antenna #1 and antenna #2 can be written as follows:

$$f_1^{\mathrm{TR}}(t) = x(-t) * H_1(-t) * H_1(t), \tag{9}$$

$$f_2^{\mathrm{TR}}(t) = x(-t) * H_1(-t) * H_2(t), \tag{10}$$

where $*$ denotes the convolution, $x(t)$ is the test signal emitted by the TRM antenna, $H_1(t)$ is the channel impulse response between antenna #1 and the TRM antenna, $H_2(t)$ is the channel impulse response between antenna #2 and the TRM antenna, and $x(-t) * H_1(-t)$ is the time-reversed signal, retransmitted from the TRM antenna. $H_1(t)$ and $H_2(t)$ can be expressed as

$$H_1(t) = \sum_{k=1}^{K} a_k \delta(t - \tau_k), \tag{11}$$

$$H_2(t) = \sum_{m=1}^{M} b_m \delta(t - \tau_m). \tag{12}$$

Substituting Eqs. (11) and (12) into Eqs. (9) and (10), we can obtain the following expressions:

$$f_1^{\mathrm{TR}}(t) = x(-t) * \left[\sum_{k=1}^{K} a_k^2 \delta(t) + \sum_{k=1}^{K} \sum_{j=1 \cup j \neq k}^{K} a_k a_j \delta(t + \tau_k - \tau_j) \right], \tag{13}$$

$$f_2^{\mathrm{TR}}(t) = x(-t) * \left[\sum_{k=1}^{K} \sum_{m=1}^{M} a_k b_m \delta(t + \tau_k - \tau_m) \right]. \tag{14}$$

As can be seen from Eqs. (13) and (14), the imaging resolution of the subwavelength array ultimately depends on the difference between the two channel responses. The greater the difference of the channel responses, the higher the resolution will be. Specifically speaking, if the multipath delays τ_k and τ_m of the two channel impulse responses are quite different from each other, the value of $f_2^{\mathrm{TR}}(t)$ in Eq. (14) will become smaller. The metamaterial sheets improve the imaging resolution of the subwavelength array by exactly increasing the difference between the channels, or in other words, by weakening the correlation among the channels.

5. Conclusions

In this paper, split-ring-based metamaterial sheets, which are employed to obtain far-field subwavelength focusing with the aid of the TR technique, are presented. The effect of the proposed metamaterial sheets is verified in experiment. The experimental results demonstrate that the split-ring-based metamaterial sheets can efficiently reduce the correlation among the channel responses of the subwavelength array elements. This split-ring-based metamaterial sheet is easy to fabricate and would find its usage in high-resolution imaging and MIMO communication systems.

References

[1] Pendry J B 2000 *Phys. Rev. Lett.* **85** 3966
[2] Shelby R A, Smith D R and Schultz S 2001 *Science* **292** 77
[3] Ibraheema I A and Koch M 2007 *Appl. Phys. Lett.* **91** 113517
[4] Grbic A and Eleftheriades G V 2002 *Appl. Phys.* **92** 5930
[5] Freire M J, Algarin J M, Behr V C, Jakob P M and Marqués R 2011 *Appl. Phys. Lett.* **98** 133508
[6] Grbic A, Jiang L and Merlin R 2008 *Science* **320** 511
[7] Belov P A, Palikaras G K, Zhao Y, Rahman A, Simovski C R, Hao Y and Parini1 C 2010 *Appl. Phys. Lett.* **97** 191905
[8] Belov P A, Hao Y and Sudhakaran S 2006 *Phys. Rev. Lett.* **73** 033108
[9] Zhou H C, Wang B Z, Ding S and Ou H Y 2013 *Acta Phys. Sin.* **62** 114101 (in Chinese)
[10] Ding S, Wang B Z, Ge G D, Zheng G and Liu X F 2010 *Conference on 2010 Microwave and Millimeter Wave Technology*, May 8–12, 2010, Chengdu, China, p. 1160
[11] Pendry J B 2008 *Science* **322** 71
[12] Fusco V, Buchanan N and Malyuskin O 2010 *IEEE Trans. Anten. Propag.* **58** 798
[13] Lerosey G, Rosny J, Tourin A and Fink M 2007 *Science* **315** 1119
[14] Ge G D, Wang B Z, Huang H Y and Zheng G 2009 *Acta Phys. Sin.* **58** 8249 (in Chinese)
[15] Chen Y M, Wang B Z and Ge G D 2012 *Acta Phys. Sin.* **61** 024101 (in Chinese)
[16] Zhang Z M, Wang B Z, Ge G D, Liang M S and Ding S 2012 *Acta Phys. Sin.* **61** 098401 (in Chinese)
[17] Ding S, Wang B Z, Ge G D, Wang D and Zhao D S 2011 *Acta Phys. Sin.* **60** 104101 (in Chinese)
[18] Zhang H Y, Cao Y P, Sun X L, Chen X H and Yu J B 2010 *Chin. Phys. B* **19** 114301
[19] Ying Y Z, Ma L and Guo S M 2011 *Chin. Phys. B* **20** 054301
[20] Ge G D, Wang B Z, Wang D, Zhao D S and Ding S 2011 *IEEE Trans. Anten. Propag.* **99** 1731
[21] Liang M S, Wang B Z, Zhang Z M, Ding S and Zang R 2013 *Acta Phys. Sin.* **62** 058401 (in Chinese)
[22] Liu X, Wang B Z, Xiao S and Lai S 2010 *IEEE Trans. Anten. Propag.* **58** 1731